

Periodic forcing in viscous fingering of a nematic liquid crystal

R. Folch^a, T. Tóth-Katona^b, Á. Buka^b, J. Casademunt^a and A. Hernández-Machado^a

^a Departament d'Estructura i Constituents de la Matèria, Universitat de Barcelona,
Avinyuda Diagonal, 647, E-08028-Barcelona, Spain

^b Research Institute for Solid State Physics and Optics, Hungarian Academy of Sciences,
H-1525 Budapest, P.O.B.49, Hungary
(February 18, 2019)

Abstract

We study viscous fingering of an air – nematic interface in a radial Hele-Shaw cell when periodically switching on and off an electric field, which reorients the nematic and thus changes the viscosity, the surface tension, and its anisotropy (mainly enforced by a single groove in the cell). We observe lateral undulations in the fingers which correlate with the switching frequency, as well as with tip oscillations which give maximal velocity to smallest curvatures. These oscillations appear to be decoupled from spontaneous (noise-induced) side branching. We conclude that the lateral undulations are generated by successive relaxations between two limiting patterns. The change between these two selected patterns is mainly due to the change in the anisotropy. This scenario is confirmed by numerical simulations in the strip geometry, using a phase-field model for anisotropic viscous fingering.

PACS number(s): 47.54.+r, 47.20.Ma, 61.30.-v, 47.20.Hw

I. INTRODUCTION

A great deal of experimental and theoretical works have been devoted to the Saffman-Taylor problem, i.e., to the destabilization of the interface between two immiscible fluids when the less viscous fluid displaces the more viscous one under pressure —for a review see [1].

Experimental results agree well with the linear stability analysis for the first destabilization of the circular interface [2]. The later stages of the interface growth in the radial geometry (after breakup of the initial circle) are less understood than those of the channel flow. For isotropic fluids the pattern continues to evolve through repeated tip-splitting to form more and more fingers.

An external perturbation, however, can change dramatically the Saffman-Taylor finger and can even suppress the tip-splitting process. A bubble of gas trapped just in front of an advancing finger causes tip stabilization and (eventually) resonant dendritic growth with intensive and very regular side branching both in the radial [3] and linear [4] geometries. Patterns grown in radial cells with a single groove running from the center to the edge of the cell went through a repeated tip-splitting process in all directions except that of the groove [5]. In the direction of the groove a much faster growing dendritic structure has been observed and the whole pattern was very similar to that reported in [3]. Engraving a grid on one of the plates of the cell also introduces an anisotropy, which, if strong enough, can inhibit tip splitting and produce dendrites and faceted structures, resulting in a rich morphology diagram [6,7]. A series of experiments over etched lattices gave a variety of highly branched structures whose symmetry depended on the symmetry of the lattice at high anisotropy [8]. The replacement of the grid lattice by a set of parallel grooves [9] has produced even a more complicated morphology diagram than that presented in [6]. An intrinsic anisotropy, such as that of a liquid crystal used as the more viscous fluid, has also been shown to stabilize the tip (prevent the tip splitting) and produce stable dendritic growth with side branches [10,11]. All these experiments have demonstrated that anisotropy can stabilize finger tips, so that, if the natural noise is strong enough, destabilization of the finger takes place only at its sides in the form of side branches.

In the channel geometry, Rabaud et. al. have taken advantage of the fact that fingers remain stable up to higher capillary numbers once anisotropy has suppressed tip splitting, to artificially induce side branching by means of an external perturbation [12]. They obtain side branches using a localized disturbance, namely a knot on the thread which provides the anisotropy. Pressure modulation also causes side branching in the case of a thread, since, according to them, it mainly induces localized initial disturbances near the intersection of the interface with the thread. In contrast, in the case of two opposite grooves in the middle of the channel, the lateral waves caused by such sinusoidal pressure oscillations (periodic forcing) are symmetrical, and, most significantly, of limited amplitude.

We investigate the formation of lateral undulations in an air finger invading a liquid crystal in the radial geometry, where the boundary conditions do not limit their amplitude, when periodically forcing the system by a gated electric field perpendicular to the cell. A single groove running over the injection point stabilizes the finger tips in its direction. The nematic director (which describes the orientation of the nematic phase) tends to align with the electric field when this is switched on, and is returned roughly to the cell plane by the

flow when this is switched off. The flow properties depend on the orientation of the director, so that we expect to change the control parameters of the dynamics whenever we switch the field on or off. The use of a square wave for the amplitude of the electric field (switching it on and off instantly) introduces more modes than a simple sinusoidal wave for it, but it enables us to watch the relaxation of the tip to a parameter quench.

We find the tip radius to relax very quickly to two different values when the field is switched on and off, and that it is this pulsating tip what induces the symmetrical lateral undulations. Finally, we explain these lateral undulations as a periodic change in the selected tip radius, mainly due to the change in the effective anisotropy introduced by the groove. Back to the linear geometry, we confirm this scenario with numerical integration of a phase-field model for viscous fingering [13] in which anisotropy is switched between two different values. Here, the alternate relaxation toward two different selected patterns is particularly clear, since the symmetrical lateral undulations saturate, as the finger oscillates between two different selected widths. These observations resemble those for a finger in the linear geometry perturbed by a bubble on its tip, in which the tip curvature oscillates and the lateral undulations are also found to be symmetrical and to lie between two well-defined asymptotic widths [12].

The rest of the paper is organized as follows: In Sec. II we present the flow properties of a nematic liquid crystal under an AC electric field, the specific setup of our experiments, and the experimental results. Sec. III then introduces and exploits the theoretical framework within which we explain the experimental observations, and Sec. IV, the numerical method for checking the outcoming hypothesis in the linear geometry, as it is needed. The conclusions reached are summarized in Sec. V.

II. EXPERIMENTAL SETUP AND RESULTS

In nematic liquid crystals the director field \vec{n} and the velocity \vec{v} are coupled by nonlinear nematohydrodynamic equations – see e.g. [14,15]. Using a nematic liquid crystal with positive dielectric anisotropy $\varepsilon_a = \varepsilon_{\parallel} - \varepsilon_{\perp} > 0$ (ε_{\parallel} and ε_{\perp} are components of the uniaxial dielectric tensor parallel and perpendicular to \vec{n} , respectively), and applying an appropriate AC electric field E perpendicular to the plane of the sample, the effective viscosity μ and the surface free energy σ should change depending on the excess pressure p_e and on E . When the shear torque [15] exerted on the director is much larger than the electric torque (high p_e and low E —hereafter E off—, elastic torques are negligible in our case) one has $\mu = \mu_1 (\approx \eta_1)$ and $\sigma \approx \sigma_{\perp}$ (if one assumes flow alignment, so that the director be parallel to the shear plane, and the molecules aligned perpendicular to the interface). In the opposite case, when the electric torque is much larger than the shear torque (hereafter E on), \vec{n} is perpendicular to the plane of the cell and we have $\mu = \mu_2 (\approx \eta_2)$ and $\sigma \approx \sigma_{\parallel}$ (here η_1 and η_2 are the corresponding Miebowicz viscosity coefficients [15], and σ_{\parallel} and σ_{\perp} are the surface free energies of an interface parallel and perpendicular to \vec{n} , respectively). Accordingly, in the experiments μ and σ should change in the range of $\mu_1 \leq \mu \leq \mu_2$ and $\sigma_{\parallel} \leq \sigma \leq \sigma_{\perp}$.

In the experiments, the commercial liquid crystal mixture RO-TN-430 (La Roche) was used, having positive dielectric anisotropy $\varepsilon_a = 17.6$, and a broad temperature range of the nematic phase (from $T_m = -10^{\circ}\text{C}$ up to $T_{N \rightarrow I} = 70^{\circ}\text{C}$). The liquid crystal mixture was

doped with dichroic blue dye D16 (BDH) in order to enhance the contrast at the air–nematic interface. The experiments were performed at room temperature $T = 23^\circ C$.

The radial Hele-Shaw cell was assembled from two glass plates, both coated with a conducting layer of SnO_2 which served as electrode. The bottom plate, of dimensions $(160\text{mm} \times 160\text{mm})$ and thickness 5.5mm in the center, had a hole of 1mm diameter as an inlet for the air. On the upper plate $(140\text{mm} \times 140\text{mm}$ and thickness 3.1mm) we made a groove running along its diagonal in order to stabilize the finger tips and obtain long enough fingers in its direction. The glass plates were separated by $d = 0.32\text{mm}$ or $d = 0.19\text{mm}$ thick spacers. The different cell thicknesses imposed different external anisotropies to the system due to the presence of the groove (smaller d means higher anisotropy).

After filtration of the air, p_e was regulated by a ported precision regulator (Norgren 11-818-100) with an accuracy of $\pm 0.03\text{bar}$. We also used a unit for pressure reduction which further decreased the pressure and enhanced its stability. The path of the air was regulated by two 3-path solenoid valves. p_e was measured by a precision pressure meter (Watson&Smith), with an accuracy of $\pm 1\text{mbar}$. An AC electric field of frequency 1kHz was applied, modulated (switched on/off) by a frequency ν . In all the experiments presented here, a filling coefficient of $\xi = t_{on}\nu = 0.67 \pm 0.03$ was used, where t_{on} denotes the time within a period during which E was on. The recorded images of the growth processes were fed into a PC for digital analysis, with a spatial resolution of $512 \text{ pixels} \times 512 \text{ pixels}$ and a 256 gray scale for each pixel. With the magnification used in the experiments, a spatial resolution of $(0.241\text{mm} \times 0.166\text{mm})/\text{pixel}$ was determined.

At low excess pressures p_e (low driving forces) the two stable viscous fingers running in the direction determined by the groove do not show any lateral undulations with E off or E on – Figs. 1(a) and 1(b), respectively. The only difference between the morphologies presented in Figs. 1(a) and 1(b) is that, with E on, the tips become narrower compared to the case with E off. Moreover, the velocity of the tip is smaller with E on due to the increase of the effective viscosity – compare the times indicated in the figure caption. However, for E modulated with a frequency ν , the tip goes through successive curvature changes which induce formation of lateral undulations in a strong correlation with the forcing frequency ν as shown in Figs. 1(c) and 1(d).

Similarly to the dendritic growth of the nematic – smectic B interface reported in [16], an upper frequency ν_c is observed for a given p_e , above which the main fingers do not show any lateral undulations — the interface cannot follow such a high forcing frequency. Fig. 1(e) illustrates this effect for $\nu > \nu_c$, showing fingers with no lateral undulations having a width smaller than that in Fig. 1(a) (E off), but larger than that in Fig. 1(b) (E on).

Oscillations in the tip velocity have also been detected for the case of a periodic forcing. Fig. 2 gives the position of the tip vs. time for the fingers shown in Fig. 1(a)–(e). As it can be seen, fingers grow much faster with E off (wider fingers) than with E on (thinner fingers). For forcing frequencies $\nu = 0.66\text{Hz}$ and $\nu = 1.01\text{Hz}$ the tip velocity oscillates in time between the values corresponding to E off and on. Weak velocity oscillations have been measured even for $\nu > \nu_c$, where no lateral undulations occurred — see the $\nu = 4.55\text{Hz}$ case in Fig. 2.

Changing the cell thickness to $d = 190\mu\text{m}$, results are similar to Fig. 1, but the width of the tip becomes smaller due to the increased anisotropy imposed by the groove – compare Figs. 1(a) and 3(a) for E off, as well as Figs. 1(b) and 3(b) for E on.

At higher p_e the main tips show a weak, uncorrelated side-branching both with E off and E on [Figs. 4(a) and 4(b), respectively], as a consequence of noise amplification. Modulation of E with a frequency ν here leads again to successive curvature changes in strong correlation with ν – see Fig. 4(c).

The upper frequency ν_c has also been observed for the higher p_e , above which the noise-induced side branches [as in Figs. 4(a) and 4(b)] reappeared. This frequency ν_c showed a roughly linear dependence on p_e .

III. THEORETICAL ANALYSIS

We now discuss a possible simplified theoretical framework to explain the experimental observations. When the electric field is off, the flow forces the director to be roughly in the plane of the cell (planar alignment). In this case the viscosity is anisotropic in the shear plane: it is lower in the direction of the director and higher in the perpendicular direction. This property, together with the fact that the director aligns itself with the flow velocity in a certain pressure range, gives rise to anisotropy in the flow, which, if strong enough, has been seen to stabilize the finger tips, thus switching from a tip-splitting to a side-branching mode [10]. This can be understood by mapping this anisotropy in the viscosity to an effective anisotropy in the surface tension [11].

However, experiments performed without any groove showed this anisotropy in the viscosity not to be strong enough to stabilize the finger tips for the liquid crystal mixture used here [17]. Therefore, as a first approximation, we will consider this planar alignment case to have an isotropic, average viscosity μ_1 .

Thus, the theoretical framework will be that of the standard viscous fingering equations, except for the dimensionless surface tension $B_0 \equiv \sigma/(p_e l_c)$ (with l_c an arbitrary length scale), which will read

$$B = B_0 \left(1 - \alpha \cos^2 \phi\right), \quad (3.1)$$

where ϕ will be the angle between the single groove used in the experiments and the normal to the interface, and α represents the two-fold anisotropy induced by the groove. Grooves and grids have usually been modeled by such an anisotropy in the surface tension (see, e.g., Ref. [18]). This represents a strong simplification, but we do not expect it to affect the conclusions of this paper in any fundamental way.

When the electric field is switched on, it forces the director to be perpendicular to the cell plane (homeotropic alignment). The viscosity in the plane of the cell is now completely isotropic, so that we can still use the same theoretical model as for the planar case. However, this isotropic viscosity μ_2 turns out to be much higher than for the planar alignment, $\mu_2 \gg \mu_1$. The viscosity μ enters the equations for a constant injection pressure p_e only through the time scale of the dynamics, $12\mu l_c^2/(d^2 p_e)$. Thus, a higher viscosity implies a slower dynamics. This explains why the interface grows more slowly when the field is on [compare Figs. 1(a) and 1(b) and the filled and empty circles in Fig. 2], but it cannot explain why fingers are also thinner. The latter should be understood as a decrease in the selected length scale for the finger tip radius for a given length of the finger, which results in a visually overall thinner finger. (Thus we will talk about thinner and wider fingers to refer to larger and smaller tip curvatures at a given finger length, respectively).

In our model, this could be due to either a decrease in the dimensionless surface tension B_0 or an increase in its anisotropy α . Indeed, Ref. [19] reports measurements of the surface tension of the nematic–air interface for several liquid crystals with the director parallel to the interface (i.e., perpendicular to the glass plates), σ_{\parallel} , and perpendicular to it (but in the plane of the cell), σ_{\perp} , and gives a decrease from σ_{\perp} (which would correspond to E off) to σ_{\parallel} (which would correspond to E on) in the range 20–50% for different substances.

It is also reasonable to believe that the interaction between the liquid crystal and the glass plates, and especially with the groove, should depend on the orientation of the director, which could then affect the effective anisotropy α due to the groove. α could also be affected by the fact that the electrodes were removed from the etched region when ruling the groove. Thus, the orientation of the nematic inside the groove could remain planar even when the field is switched on, so that the lower viscosity associated to the planar alignment would give an even higher mobility inside the groove, thus reinforcing the mobility enhancement of the groove itself (higher gap d), and therefore increasing the effect of the groove (the anisotropy α in our model).

To check the different possibilities, we decreased the cell gap d , which is the standard way of increasing the effect of a groove or grid [6,18], and which does not affect anything else in our model but the time scale. Fig. 3 shows fingers grown with this lower gap. The fact that the fingers in Figs. 1(b) and 3(a) have very similar widths shows that the same narrowing of the finger can be achieved either by switching on the field or increasing α through a decrease in d . This supports the hypothesis that the electric field increases α . The anisotropy can still be further increased by switching on the field with this lower cell gap d , and the finger narrows more [Fig. 2(b)].

Then, we kept this lower cell gap and increased the injection pressure up to $p_e = 22\text{mbar}$ (Fig. 4), in order to decrease the dimensionless surface tension B_0 . This was clearly achieved, since the interfaces in Fig. 4 are much noisier, and the fingers growing perpendicular to the groove even tip-split. (The amount of noise necessary for a finger to tip-split is known to decrease with decreasing dimensionless surface tension [20]). However, there is no significant width change with increasing p_e , as can be seen by comparing Figs. 3(a) and 3(b) with Figs. 4(a) and 4(b), respectively. Since the change in surface tension measured for other liquid crystals (typically 30%) would cause a smaller change in the dimensionless surface tension B_0 than changing p_e from 5mbar to 22mbar , we are led to conclude that it is the anisotropy in the surface tension and not the dimensionless surface tension itself what accounts for the observed width change.

On the other hand, it is well known that a thinner finger grows faster in dimensionless time, although the experimental observation is just the opposite in real time. This means that the change in the time scale due to the change in the viscosity is also necessary to account for the experimental observations, and indeed must be dominant over the change in dimensionless time. The change in the time scale was measured from the growth of a circular interface in the absence of grooves with the field on and off, and we found that the time scale is a factor $\mu_2/\mu_1 = 3.7$ slower when the field is on. Now, the question is whether there is a range of change of α which gives the observed narrowing of the finger but also respects the fact that thinner fingers actually grow slower. To answer this question we numerically integrate the described theoretical model, but we run it in the channel geometry. The method, which will also help us check the theoretical scenario for the lateral undulations

observed when gating the field, is described in the following section.

IV. NUMERICAL RESULTS AND DISCUSSION

We use the phase-field model for viscous fingering presented and tested in Ref. [13]. The only change in the model is that we now use the anisotropic surface tension given by Eq. (3.1). We recall the mentioned model,

$$\tilde{\epsilon} \frac{\partial \psi}{\partial t} = \nabla^2 \psi + c \vec{\nabla} \cdot (\theta \vec{\nabla} \psi) + \frac{1}{\epsilon} \frac{1}{2\sqrt{2}} \gamma(\theta) (1 - \theta^2) \quad (4.1)$$

$$\epsilon^2 \frac{\partial \theta}{\partial t} = f(\theta) + \epsilon^2 \nabla^2 \theta + \epsilon^2 \kappa(\theta) |\vec{\nabla} \theta| + \epsilon^2 \hat{z} \cdot (\vec{\nabla} \psi \times \vec{\nabla} \theta), \quad (4.2)$$

where ψ is the stream function, $c \equiv (\mu - \mu_0)/(\mu + \mu_0)$ is the viscosity contrast (μ, μ_0 are the viscosities of the liquid crystal and the air, respectively), θ is the phase field, and $\epsilon, \tilde{\epsilon}$ are model parameters which must be small to recover the sharp-interface equations of the theoretical model. We have defined $f(\theta) \equiv \theta(1 - \theta^2)$, and $\frac{\gamma(\theta)}{2} \equiv \hat{s}(\theta) \cdot [\vec{\nabla} B(\theta) \kappa(\theta) + \hat{y}]$, $\kappa(\theta) \equiv -\vec{\nabla} \cdot \hat{r}(\theta)$, with $\hat{r}(\theta) \equiv \vec{\nabla} \theta / |\vec{\nabla} \theta|$ and $\hat{s}(\theta) \equiv \hat{r}(\theta) \times \hat{z}$. All quantities are dimensionless and, in particular, lengths are in units of the channel width (y is length along the channel and x across it).

We set $B_0 = 10^{-2}$, which we know to allow stable fingers for the amount of numerical noise present even for vanishing anisotropy [11]. We use two different values of the anisotropy, $\alpha = 0.9$ and $\alpha = 0.1$, to account for the cases with and without electric field, respectively. The higher anisotropy gives the lowest B at the finger tip which we will need to resolve, and thus the value of the interface width to use, $\epsilon = 0.00625$. As for the viscosity contrast, for numerical convenience we use $c = 0.9$, which is known (see, e.g., Ref. [11]) to be sufficiently close to the high viscosity contrast limit $c = 1$ of the experiments. $\tilde{\epsilon} = 0.4$, which suffices to resolve the displacement of the liquid crystal by the air. The initial condition is a cosine wave of wavelength and amplitude 1 (the channel width) in all cases.

Since the runs use dimensionless variables, the effect of the different time scale with or without the electric field does not show up. To make it apparent, we introduce another dimensionless time increment,

$$\Delta t' \equiv \begin{cases} \Delta t & \text{when field is off} \\ \frac{\mu_2}{\mu_1} \Delta t & \text{when field is on,} \end{cases} \quad (4.3)$$

and we compare runs at a same time t' . In this way we compare runs which would have taken the same time in the experiments, since the factor restoring the dimensions is now the same independently of how much time was the field on or off during each run. Also, the phase-field equations [(4.1) and (4.2)] are in the reference frame moving with the mean interface. Since the experimental figures are in the lab frame, the runs have been translated into the latter.

In Fig. 5(a) we show a wider ($\alpha = 0.1$, field off, $\lambda = 0.588$) and thinner ($\alpha = 0.9$, field on, $\lambda = 0.387$) finger, both at $t' = 7.8$, where λ is the finger width. We can see that the

wider finger does go faster even with this enormous change in α . Therefore, we conclude that a simultaneous increase in the surface tension anisotropy and the viscosity, does actually explain the fact that fingers are both narrower and slower.

Once we have understood how the introduction of an electric field affects the width and velocity of the fingers, we are in a position to explain the experimental observations when the electric field is periodically switched on and off. One would be tempted to understand the lateral oscillations in Figs. 1(c), 1(d) and 4(c) as standard (noise-induced) side branches, amplified and regularized by some resonance phenomenon with the oscillations of a control parameter, as seen in related problems [16]. In this case the relevant control parameter should be the anisotropy α , since the viscosity only enters the time scale, and can thus not affect the shape of the pattern. In this scenario, the fact that Fig. 1(e) shows no oscillations would be interpreted as the result of being too far from the resonance frequency, and the velocity oscillations seen in Fig. 2 would be those sometimes associated with side branching.

However, the velocity turns out to decrease when the finger tip narrows, as opposite to the usual case, so that the velocity oscillations must be due to the periodic change in the time scale and not a signal of genuine side branching. The fact that the finger tip narrows exactly when the field is switched on and widens when it is switched off suggests that the mentioned lateral oscillations have nothing to do with noise-induced side branching either, but are just the wake left by the successive selected tip curvatures with and without electric field.

In contrast, Figs. 4(a) and 4(b) show spontaneous, noise induced side branching, since here the field is held on or off during the whole growth process. Thus, Fig. 4(c) shows the superimposition of the mentioned wake of periodic width changes due to switching on and off the field and the spontaneous side-branching. There seems to be no significant coupling between the two effects, which supports the idea that the oscillations in Figs. 1(c), 1(d) are the result of relaxation back and forth between two widths. In this new picture, Fig. 1(e) shows no width oscillations because the frequency is too high for the width to relax to those in Figs. 1(a) and 1(b), but should present an intermediate width, as seems to be the case.

The problem here is that anisotropic viscous fingers in the circular geometry do not reach a steady tip radius nor velocity. There is indeed a selection mechanism, but the first keeps growing and the latter decreasing with time (see Ref. [21]). Therefore, it is especially useful to run anisotropic fingers in a channel to check out this scenario, since their widths and velocities do saturate and are easy to compare with one another. In this way, Figs. 5 and 7 are the computational, channel analogues of Figs. 1 and 2, obtained from experiments in the circular geometry.

In Figs. 5(b) and 5(c) interfaces are shown exactly each time the anisotropy was changed between the two different values in Fig. 4(a) (whenever the field was switched on or off), which was done with a very similar filling coefficient than in the experiments, $\xi = 0.67$. This visually leaves no doubt of the fact that the two different widths in Fig. 5(a) are successively selected at the tip to produce the pattern in Fig. 5(b). The small mismatch between the tails of the two front interfaces in Fig. 5(b) is presumably due to the fact that the viscosity contrast is not strictly 1 ($c = 0.9$), so that the dynamics in the tail region is not completely frozen. In Fig. 5(c) the width has no time to relax to any of the two in Fig. 5(a), and gently oscillates in the intermediate range $0.526 < \lambda < 0.537$. However, the curvature seems to relax more quickly.

These relaxation processes can be seen in more detail in Fig. 6, where we have monitored the finger width one unit length behind the tip (which is only slightly below the asymptotic width) and the tip radius. The latter is the inverse of the curvature modulus of the zero level-set of the phase field ($1/|\kappa(\theta = 0)|$), and therefore of the interface. To avoid lattice oscillations, such a radius is plotted only when the finger tip hits near a grid point ($|\theta| < 10^{-3}$ at the tip of the finger). The solid and dashed lines correspond to the runs in Fig. 5 (b) and 5 (c) respectively. In the case of the lower frequency (solid lines), we can see that the tip radius relaxes always first to its asymptotic value, and is then followed by the finger width as the information of the tip is left behind. Thus, for the higher frequency (dashed lines), the finger has not enough time to relax to its asymptotic widths, but the curvature almost attains its asymptotic values. On the other hand, for the lower frequency it is possible to observe that the tip widens much faster than it narrows, as can be seen both in the tip width and its radius, but especially in the first. This behavior may be expected in connection with the existence of a set of (unstable) solutions with larger width than the selected one, whose proximity may effectively slow down the relaxation dynamics.

Finally, in Fig. 7 we show the evolution of the tip position for the runs in Fig. 5. The steeper (less steep) straight, long-dashed line corresponds to the wider (thinner) finger in Fig. 5 (a), i.e. to the case with the field off (on). The initial relaxation to the stationary velocity is so fast that it is almost invisible at this scale. The runs in Figs. 5 (b) and (c) correspond to the solid and dotted lines in between respectively. We can see that, for the lower frequency (solid line), the velocity successively relaxes to the values with or without field of the straight, long-dashed lines. Initially, however, it attains a value slightly below (above) the steady velocity when it relaxes to a lower (higher) velocity. This effect is more apparent for the relaxation to a lower velocity. In contrast, for the higher frequency (dotted line), we are left with these initial slightly too low or high values of the velocity, since the field is switched on or off again just when the velocity was about to achieve its asymptotic value. This is quite similar to what happened to the curvature for the higher frequency (lower dashed line in Fig. 6), in contrast with the failure of the finger width to relax (upper dashed line in Fig. 6). So the finger velocity seems to be more correlated to the tip curvature than to the finger width.

As a final remark, we would like to mention that we have also reproduced qualitatively Figs. 5 and 7 by changing the dimensionless surface tension from $B_0 = 10^{-2}$ to $B_0 = 6.5 \times 10^{-4}$ (with $\epsilon = 0.005$) and keeping its anisotropy to $\alpha = 1$. In the experiments of Rabaud et. al. with two opposite grooves in the linear geometry in which they modulated the pressure [12], this pressure modulation is equivalent to modulating the time scale and the dimensionless surface tension, so that these simulations describe the lateral undulations seen there (although not the time scale), and actually explain why they are found to be symmetrical and of limited amplitude. (Strictly speaking, the experiments used a sinusoidal wave, whereas the simulations use a square one).

V. CONCLUSIONS

We have performed viscous fingering experiments in a radial Hele–Shaw cell, where the more viscous fluid was a liquid crystal mixture in its nematic phase. After ruling a single groove across the center of the cell, we achieved stable finger tips in the direction of the

groove (otherwise unstable). By applying an electric field perpendicular to the cell, we oriented the nematic director in this direction, which resulted in thinner and slower fingers. We then periodically switched on and off the field to find oscillations in the finger width and velocity, with an amplitude which decreased as the frequency of switching on and off was increased.

We explain how fingers are slower when the field is on because the viscosity of the liquid crystal is higher with the director perpendicular to the cell, and we have shown by numerical integration in the channel geometry of a simplified theoretical model that the reason why they are thinner may be attributed to an increase in the anisotropy due to the groove when the field is on. Also the surface tension is reduced when the field is switched on, but it cannot affect much the finger width, since no significant width change was observed by increasing the excess pressure, and both a decrease in the surface tension and an increase in the excess pressure would lower the dimensionless surface tension. We also explain the finger width and velocity oscillations as the result of the relaxation back and forth between the selected tip curvatures and velocities with the field on and off, as suggested by the experiments and clearly seen in the numerical integration of the theoretical model.

This latter result might be relevant to the lateral undulations seen in a finger with a bubble on its tip in the linear geometry for the case of a pulsating tip curvature, since they also turn out to be symmetrical, and their envelop is a wider Saffman–Taylor finger [12].

Finally, the same width change is observed in the numerical integration of our model in the channel geometry when the dimensionless surface tension is changed keeping its anisotropy constant, which is roughly the case of a pressure modulation with two opposite grooves providing the anisotropy. Experiments with this pressure modulation also show symmetrical lateral undulations of limited amplitude [12].

ACKNOWLEDGMENTS

We acknowledge financial support from the Dirección General de Enseñanza Superior (Spain), Projects No. PB96-1001-C02-02 and PB96-0378-C02-01, from the National Scientific Research Foundation (Hungary), Grants No. OTKA F022771 and OTKA T031808, and the European Commission, Project No. ERB FMRX-CT96-0085. Simulations have been carried out using the resources at CESCA and CEPBA, coordinated by C⁴. R.F. also acknowledges a grant from the Comissionat per a Universitats i Recerca (Generalitat de Catalunya). R.F. and A.H.M wish to thank T. Tóth-Katona and Á. Buka for the invitation to the Research Institute for Solid State Physics and Optics and for their hospitality.

REFERENCES

- [1] K. McCloud and J. Maher, *Phys. Rep.* **260**, 139 (1995).
- [2] L. Paterson, *J. Fluid Mech.* **113**, 513 (1981).
- [3] Y. Couder, O. Cardoso, D. Dupuy, P. Tavernier and W. Thom, *Europhys. Lett.* **2**, 437 (1986).
- [4] Y. Couder, N. Gerard and M. Rabaud, *Phys. Rev. A* **34**, 5175 (1986).
- [5] M. Matsushita and H. Yamada, *J. Cryst. Growth* **99**, 161 (1990).
- [6] E. Ben-Jacob, R. Godbey, N. Goldenfeld, J. Koplik, H. Levine, T. Müller and L. Sander, *Phys. Rev. Lett.* **55**, 1315 (1985).
- [7] E. Ben-Jacob and P. Garik, *Nature* **343**, 523 (1990).
- [8] J. Chen and D. Wilkinson, *Phys. Rev. Lett.* **55**, 1892 (1985); J. Chen, *Experiments in Fluids* **5**, 363 (1987).
- [9] V. Horváth, T. Vicsek and J. Kertész, *Phys. Rev. A* **35**, 2353 (1987).
- [10] see e.g. Á. Buka, in *Pattern Formation in Liquid Crystals*, edited by Á. Buka and L. Kramer (Springer, New York, 1996) p. 291
- [11] R. Folch, J. Casademunt and A. Hernández-Machado, *Phys. Rev. E* **61**, 6632 (2000).
- [12] M. Rabaud, Y. Couder and N. Gerard, *Phys. Rev. A* **37**, 935 (1988).
- [13] R. Folch, J. Casademunt, A. Hernández-Machado and L. Ramírez-Piscina, *Phys. Rev. E* **60**, 1724 (1999); *ibid.* **60**, 1734 (1999).
- [14] H. Pleiner and H. Brand, in *Pattern Formation in Liquid Crystals*, edited by Á. Buka and L. Kramer (Springer, New York, 1996) p.15
- [15] E. Dubois-Violette and P. Manneville, in *Pattern Formation in Liquid Crystals*, edited by Á. Buka and L. Kramer (Springer, New York, 1996) p.91
- [16] T. Börzsönyi, T. Tóth-Katona, Á. Buka and L. Gránásy, *Phys. Rev. Lett.* **83**, 2853 (1999).
- [17] T. Tóth-Katona and Á. Buka (unpublished)
- [18] E. Ben-Jacob, P. Garik, T. Mueller and D. Grier, *Phys. Rev. A* **38**, 1370 (1988); E. Ben-Jacob and P. Garik, *Physica D* **38**, 16 (1989).
- [19] V.A. Tsvetkov, O.V. Tsvetkov and V.A. Balandin, *Mol. Cryst. Liq. Cryst.* **329**, 305 (1999).
- [20] D. Bensimon, *Phys. Rev. A* **33**, 1302 (1986).
- [21] R. Almgren, W.-S. Dai and V. Hakim, *Phys. Rev. Lett.* **71**, 3461 (1993)

FIGURE CAPTIONS

FIG. 1 Contours of the air – nematic interface taken at subsequent times on top of each other, $d = 320\mu\text{m}$, $p_e = 5\text{mbar}$. **(a)** E off, $t = 0.32s, 0.64s, 0.96s, 1.32s$; **(b)** $E = 0.32V/\mu\text{m}$ on, $t = 1.08s, 2.20s, 3.32s, 4.44s$; **(c)** modulated E , $\nu = 0.667\text{Hz}$, $\xi = 0.68$, $t = 0.4s, 1.44s, 1.84s, 2.64s$; **(d)** modulated E , $\nu = 1.01\text{Hz}$, $\xi = 0.68$, $t = 0.72s, 1.04s, 1.68s, 2.04s, 2.68s, 2.88s$; **(e)** modulated E , $\nu = 4.55\text{Hz}$, $\xi = 0.68$, $t = 0.52s, 1.04s, 1.56s, 2.08s$. Subfigures **(c)** and **(d)** show the contours when the field E is switched on/off.

FIG. 2 Tip position vs. time for the patterns shown in Fig. 1. Filled symbols denote E on, while empty symbols mean E off.

FIG. 3 Contours of the air – nematic interface taken at subsequent times on top of each other, $d = 190\mu\text{m}$, $p_e = 5\text{mbar}$. **(a)** E off, $t = 0.24s, 0.60s, 1.00s, 1.40s$; **(b)** $E = 0.55V/\mu\text{m}$ on, $t = 0.60s, 1.12s, 1.72s, 2.24s$.

FIG. 4 Contours of the air – nematic interface taken at subsequent times on top of each other, $d = 190\mu\text{m}$, $p_e = 22\text{mbar}$. **(a)** E off, $t = 0.04s, 0.12s, 0.20s, 0.24s$; **(b)** $E = 0.55V/\mu\text{m}$ on, $t = 0.08s, 0.16s, 0.28s, 0.36s$; **(c)** modulated $E = 0.58V/\mu\text{m}$, $\nu = 8.42\text{Hz}$, $\xi = 0.68$, $t = 0.12s, 0.20s, 0.28s, 0.36s$;

FIG. 5 Interfaces in the channel geometry, simulated in the reference frame moving with the mean interface and then translated into the lab frame. $B_0 = 10^{-2}$, $\epsilon = 0.00625$, $c = 0.9$, $\tilde{\epsilon} = 0.4$. (a) Change of width in the stationary pattern at $t' = 7.8$ from $\alpha = 0.1$ (wider finger) to $\alpha = 0.9$ (thinner finger). (b),(c) Periodic, instantaneous change of α between the values in (a), with a lower (b) and a higher (c) frequency. Interfaces are shown whenever the field is switched on or off with $\xi = 0.67$, until $t' = 15.3$.

FIG. 6 Finger width one unit length behind the tip and tip radius vs. rescaled time (t') for the runs in Figs. 5(b) (solid lines) and 5(c) (dashed lines). Remind that the unit length is the channel width.

FIG. 7 Tip position (y) vs. rescaled time (t') for the runs in Fig. 5. The steeper (less steep) straight, long-dashed line corresponds to the wider (thinner) finger in Fig. 5(a). The solid and dotted lines in between correspond to the runs in Figs. 5(b) and 5(c) respectively.

FIGURES

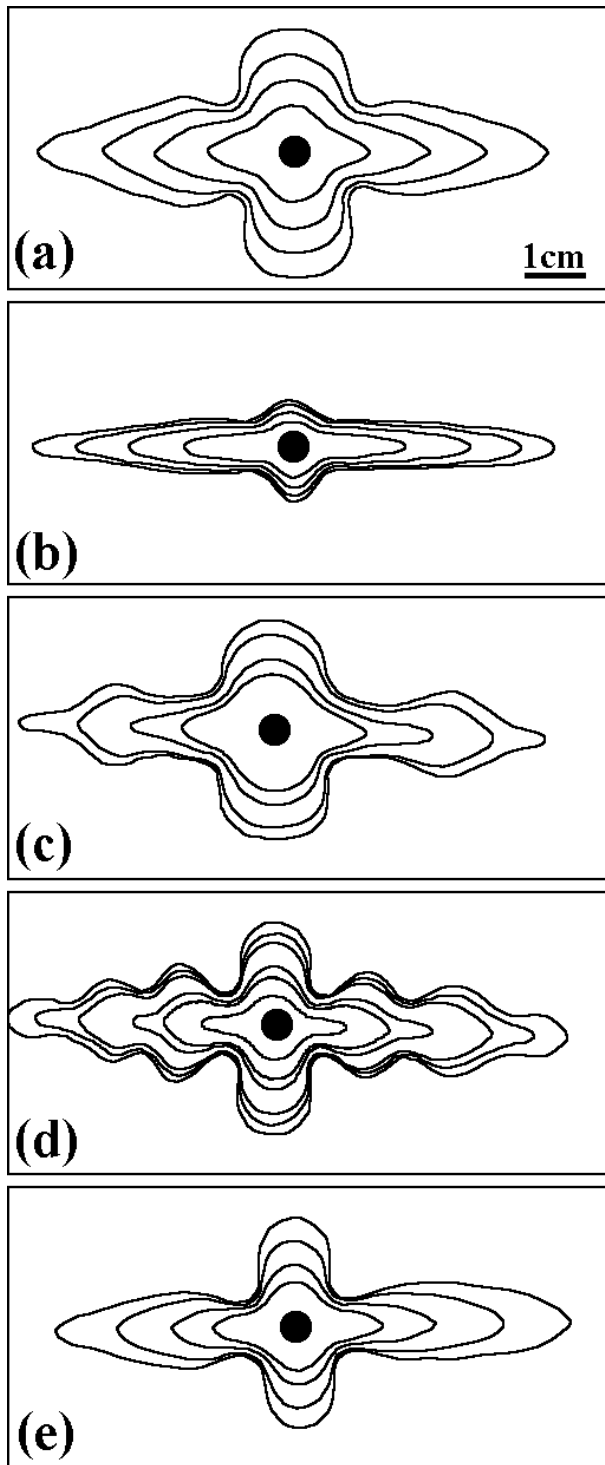


FIG. 1.

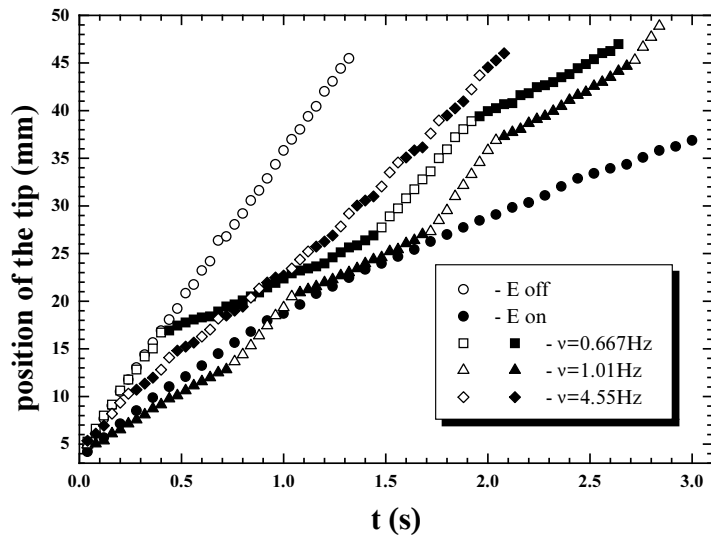


FIG. 2.

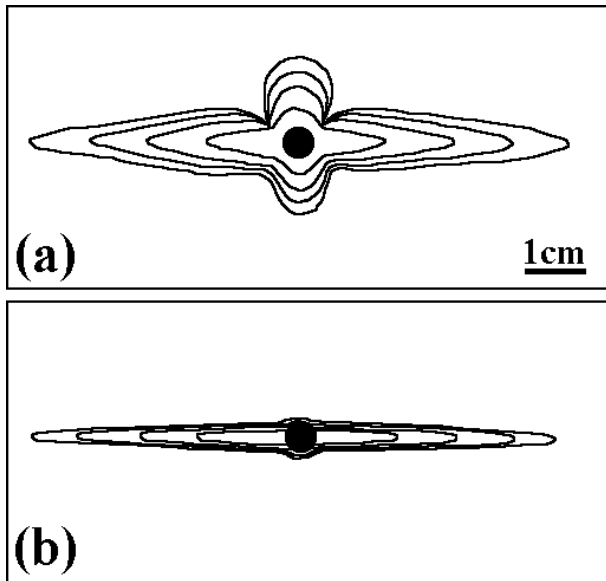


FIG. 3.

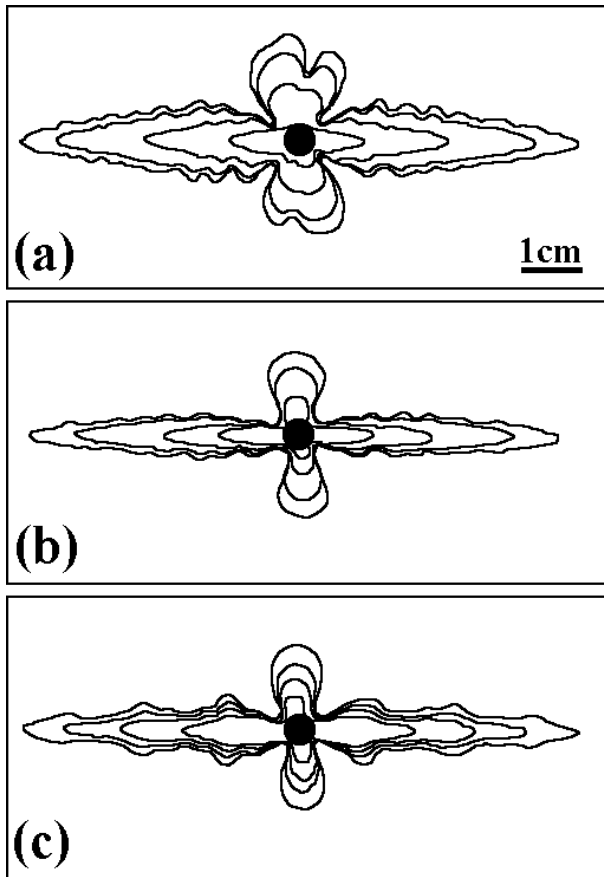


FIG. 4.

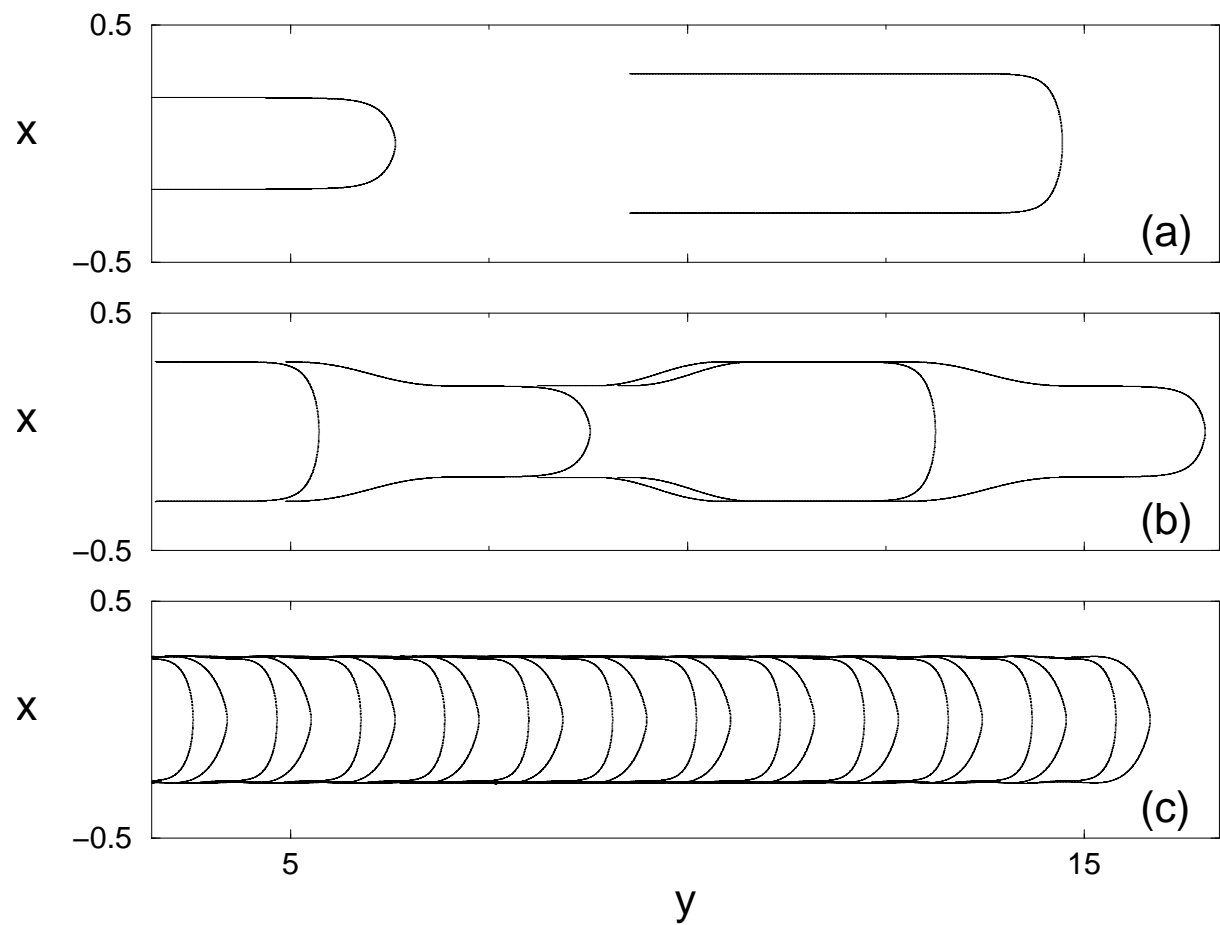
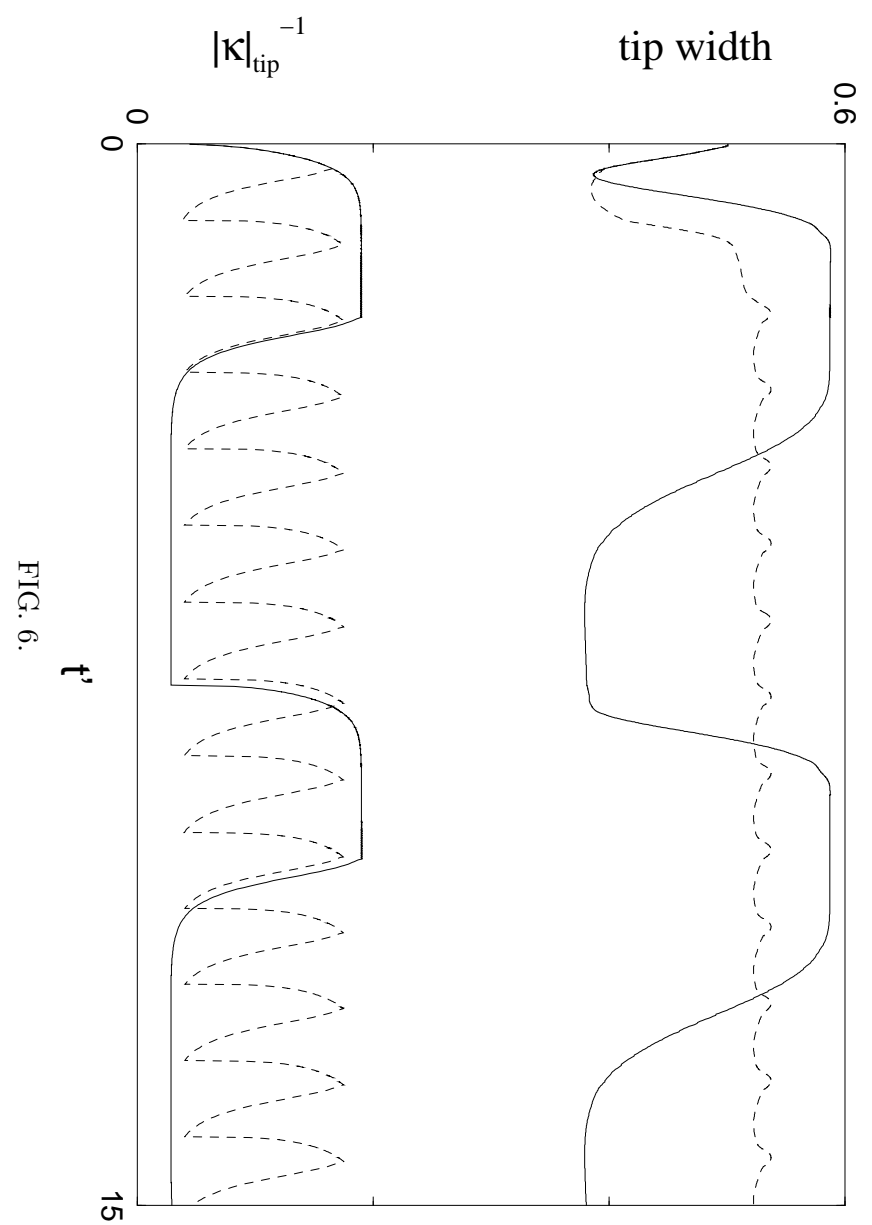


FIG. 5.



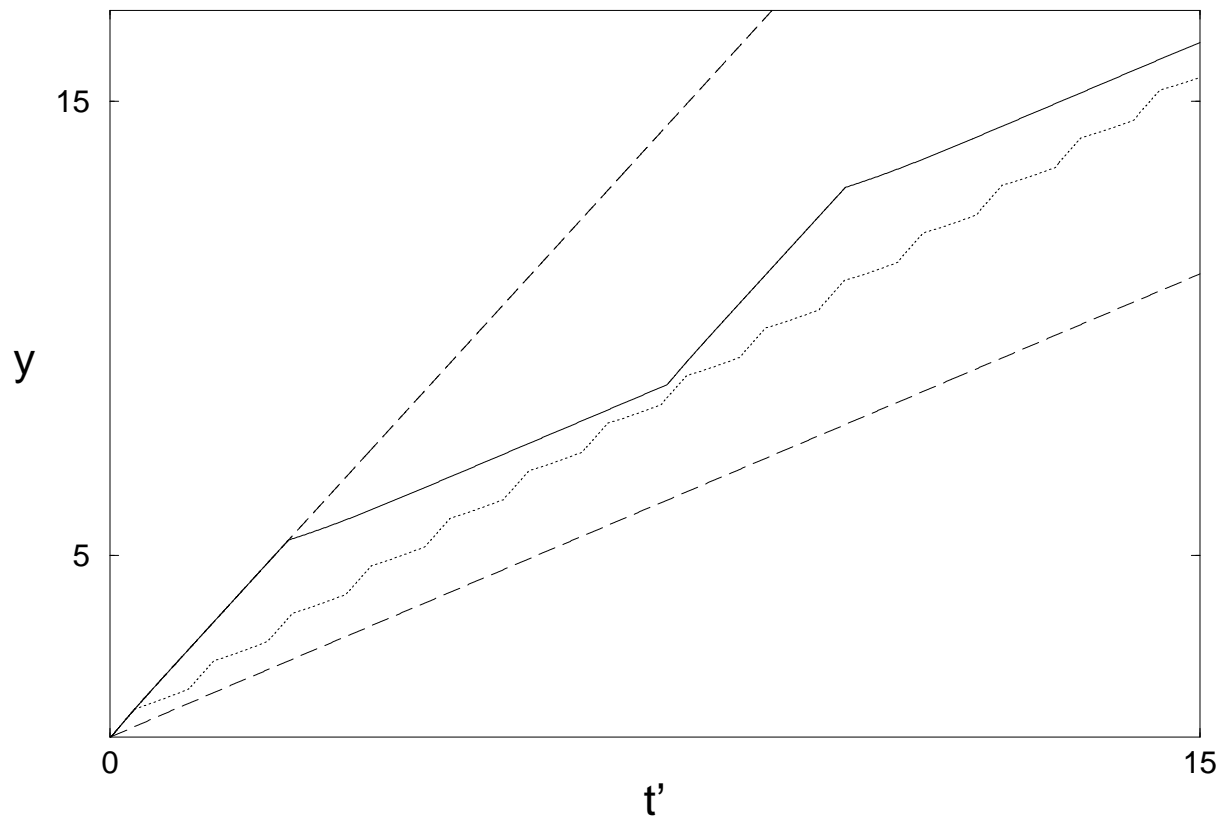


FIG. 7.